



HAL
open science

Conformational preference analysis in C₂H₆ using Orbital Forces and Non-Covalent Interactions; comparison with related systems

Patrick Chaquin, Julia Contreras-Garcia, Trinidad Novoa

► **To cite this version:**

Patrick Chaquin, Julia Contreras-Garcia, Trinidad Novoa. Conformational preference analysis in C₂H₆ using Orbital Forces and Non-Covalent Interactions; comparison with related systems. *Physical Chemistry Chemical Physics*, 2023, 25, pp.4276-4283. 10.1039/d2cp04913a . hal-03969347

HAL Id: hal-03969347

<https://hal.science/hal-03969347>

Submitted on 2 Feb 2023

HAL is a multi-disciplinary open access archive for the deposit and dissemination of scientific research documents, whether they are published or not. The documents may come from teaching and research institutions in France or abroad, or from public or private research centers.

L'archive ouverte pluridisciplinaire **HAL**, est destinée au dépôt et à la diffusion de documents scientifiques de niveau recherche, publiés ou non, émanant des établissements d'enseignement et de recherche français ou étrangers, des laboratoires publics ou privés.

Conformational preference analysis in C₂H₆ using Orbital Forces and Non-Covalent Interactions; comparison with related systems

Trinidad Novoa,¹ Julia Contreras-García,¹ Patrick Chaquin^{1,*}

¹ Laboratoire de Chimie Théorique (LCT)
Sorbonne Université, CNRS, F-75005 Paris
E-mail : chaquin@lct.jussieu.fr
Laboratoire de Chimie Théorique (LCT)
Sorbonne Université, CNRS, F-75005 Paris

Abstract

Dynamic Orbital Forces (DOF) and Non-Covalent Interactions (NCIs) are used to analyze the attractive/repulsive interactions responsible of the conformational preference of ethane and some related compounds. In ethane, it is found that the stabilization of the staggered conformation with respect to the adiabatic eclipsed one arises from both attractive and repulsive interactions in CH₃...CH₃. Attractive ones are predominant in a ratio 2:1, with an important role of a σ MO. On the contrary, the stabilization of the staggered conformation with respect to the vertical eclipsed one arises almost only from repulsive π interactions. Weak long-range H...H repulsions also favour the staggered conformation. From the sum of DOFs, yielding intrinsic bond energies, the rotation barrier can be decomposed into a weakening of the C-C bond (ca. 7 kcal/mol), moderated by a strengthening of C-H ones (ca. 4 kcal/mol). This evidences the decrease of hyperconjugation in the eclipsed conformation with respect to the staggered one. In the compounds CH₃-SiH₃, SiH₃-SiH₃, CH₃-CF₃ and CF₃-CF₃, the conformational preference is predominantly or exclusively due to repulsive interactions, with respect as well to adiabatic as to vertical eclipsed structures.

1. Introduction

The preference of ethane for the staggered (S) conformation over the eclipsed (E) one has been qualitatively explained on the basis of molecular orbital (MO) interactions between the two CH₃ groups, yielding the couple of degenerate MOs e_u,e_g and e',e'' respectively (Fig 1, see also Fig. 2 in section 3).¹ In a first step, we consider only the 4-electron interactions (a) of two CH₃ moieties leading to Pauli repulsion. Due to a smaller overlap, this interaction is globally less repulsive in S conformation. This interaction, as "steric hindrance", was for a long time considered as the only responsible of the conformational preference of ethane, as presented in most of Organic Chemistry textbooks.

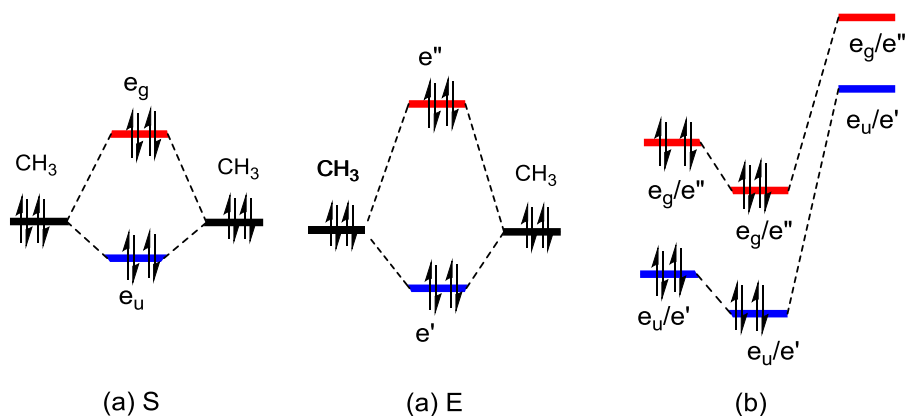


Figure 1. (a) Pauli repulsion in staggered S and eclipsed E conformations; (b) effects of hyperconjugation.

In a second step, we consider the interactions (b) of these degenerate couples with empty antibonding MOs of C-H. It results in a stabilization of both bonding (e_u , e') and antibonding (e_g , e'') MOs. Contrary to the preceding one, this interaction, also known as hyperconjugation, has a greater overlap in S which is more stabilized. The nature of the prominent interaction, Pauli repulsion vs. stabilizing hyperconjugation and, more generally, repulsive/destabilizing vs. attractive/stabilizing interactions, was the subject of many debates. Pophristic, Goodman et al., from NBO analysis, concluded that hyperconjugation was the main factor of the ethane conformational preference.² Moreover, these authors highlighted the importance of the structural changes from S to E conformer, concerning CC and also CH bonds, respectively shorter and longer in the S conformer. The study of electrostatic forces from Hellman-Feynman theorem³ or Ehrenfest forces⁴ confirmed the attractive origin of the S conformation. These conclusions were contested by several works on the basis of various energy partitions, claiming the repulsive origin of the destabilization of the E conformer with respect to the S one⁵, in turn rebutted by Weinhold.⁶ In addition, contrasted results are reported when considering either adiabatic (geometry optimized) or vertical (with the same bond lengths and angles as the S structure) geometry of the eclipsed form.⁷

We intend here to analyze the interactions leading to the preferential conformation of ethane and some compounds of general formula X_3A-BY_3 on the basis of two independent methods: dynamic orbital forces (DOF) and non-covalent interactions (NCIs).

2. Methodology

Dynamic Orbital Forces (DOF)

From generalized Koopman's theorem, the energy ε_i of a canonical MO can be written as:

$$\varepsilon_i = E^0 - E_i^+$$

where E^0 is the Hartree-Fock (H-F) energy of the determinant corresponding to the neutral molecule and E_i^+ is the energy of the determinant built with the same MOs (frozen MO approximation) in which the i^{th} MO has been removed. The derivative with respect to any internuclear distance R , after geometry optimization of the neutral species, is:

$$\frac{d\varepsilon_i}{dR} = \frac{dE^0}{dR} - \frac{dE_i^+}{dR} = -\frac{dE_i^+}{dR} \quad (1)$$

This quantity is positive or negative and represents the force exerted on nuclei upon vertical ionization from the i^{th} MO, i.e. before electron and geometry relaxation. A positive value of $\frac{d\varepsilon_i}{dR}$ means that a repulsive force is exerted in the cation and thus that the missing electron was bonding. This is a measure of the intrinsic bonding/antibonding character of each MO along R ,⁸ and was used to determine the properties of "lone pair" MOs.^{8,9}

Let us now consider the sum Σ_t over valence MOs occupied by n_i electrons:

$$\Sigma_t = \sum_i^{\text{valence}} n_i \frac{d\varepsilon_i}{dR} \quad (2)$$

This quantity has been recognized as an index of bond strength.¹⁰ Dealing with CC bonds in hydrocarbons, Σ_t was found to be linearly correlated ($r^2 = 0.96$) to intrinsic bond energy (BE) in a panel of 15 bonds,¹¹ with BE values based on AIM calculations.¹² It allowed BE evaluations in constrained systems such as propellane^{11,13} and partition into σ/π contributions to bonding.¹⁴ Then the sum Σ_t will be exploited in different ways.

(i) If n_j bonding and n_k antibonding electrons are present, the total contribution to bond strength can be decomposed into attractive Σ_b and repulsive Σ^* components:

$$\Sigma_t = \Sigma_b + \Sigma^* = \sum_j^{\text{bonding}} n_j \frac{d\varepsilon_j}{dR} + \sum_k^{\text{antibond}} n_k \frac{d\varepsilon_k}{dR} \quad (3)$$

(ii) If n_σ sigma and n_π pi electrons are present, the total contribution to bond strength can be decomposed into sigma Σ_σ and pi Σ_π components:

$$\Sigma_t = \Sigma_\sigma + \Sigma_\pi = \sum n_\sigma \frac{d\varepsilon_\sigma}{dR} + \sum n_\pi \frac{d\varepsilon_\pi}{dR} \quad (4)$$

(iii) For a small variation $\Delta\Sigma_t$ of Σ_t , one can assume the corresponding variation $\Delta(\text{BE})$ of the intrinsic bonding energy BE is:

$$\Delta(\text{BE}) \approx \text{BE} \frac{\Delta\Sigma_t}{\Sigma_t}$$

It results in a variation ΔE of the molecular energy:

$$\Delta E \approx -\text{BE} \frac{\Delta\Sigma_t}{\Sigma_t} \quad (5)$$

The canonical MOs, obtained from H-F calculations, were used in preference to Kohn-Sham (K-S) ones, provided by DFT, for different reasons. First, K-S MOs do not obey Equation 1 and their physical meaning is only the slope of their energy as a function of R. Second, more importantly, the sums of their DOF exhibit worse correlations with bonding energies.¹¹ In practice, K-S MO forces are generally quite close to H-F ones, according to the choice exchange-correlation functional.^{13,14}

Non-Covalent Interactions (NCIs)

The non-covalent interaction (NCI) index is a density (ρ) derived function enabling to reveal non-covalent interactions in real space.¹⁵

It is based on the analysis of the reduced density gradient:

$$s(\rho) = \frac{1}{2(3\pi^2)^{1/3}} \frac{|\nabla\rho|}{\rho^{4/3}}$$

It is a dimensionless quantity used in DFT to describe the deviation from a homogenous electron distribution. By plotting s isosurfaces at low electron density values, the weak interactions of the system are revealed. In order to differentiate between the different types of interactions, we will use the following colour code:

- Blue for highly attractive weak interactions (such as hydrogen bonds).
- Green for extremely weak interactions (such as van der Waals).
- Red for repulsive interactions (such as steric clashes).

3. Calculation methods

Geometry optimizations and rotation barriers were computed at the Hartree-Fock/aug-cc-pvQZ level. It has been shown that the correlation has a very weak effect on the rotation barrier of ethane.¹⁶ In

other words, the correlation energy is almost the same in the various conformations. It can be verified in Table 3, where H-F barriers differ by less than 10% (6 % for ethane) from experimental values, a sufficient precision for our purpose. Similarly, geometry parameters are very close to those obtained when correlation is included.

MO energy derivatives were computed by finite differences ranging from 0.005 Å to 0.02 Å according to the case, thanks to a home-made code (available on request). The GAUSSIAN series of programs¹⁷ was used throughout the work. NCI images were obtained with NCIPLLOT.¹⁸

4. Conformation of ethane

4.1. Orbital forces in ethane conformers

We report in Fig. 1 the DOFs of staggered S and eclipsed adiabatic E conformers in their optimized geometry (H-F/aug-cc-pvQZ, S: CC=1.524135 Å; CH = 1.083538 Å; HCC = 111.209° ; E: CC = 1.538668 Å; CH = 1.082331 Å; HCC = 111.614°), together with those of the vertical eclipsed conformer E(V) (CC, CH and HCC parameters of the S conformer). These forces correspond to the derivatives with respect to the CC distance (cf. Equation 1), the other parameters (C-H bond lengths and HCC angles) remaining unchanged. These quantities are thus a measure of the attractive (DOF > 0) or repulsive (DOF < 0) interaction of one CH₃ group with another exerted by one electron occupying a given MO.

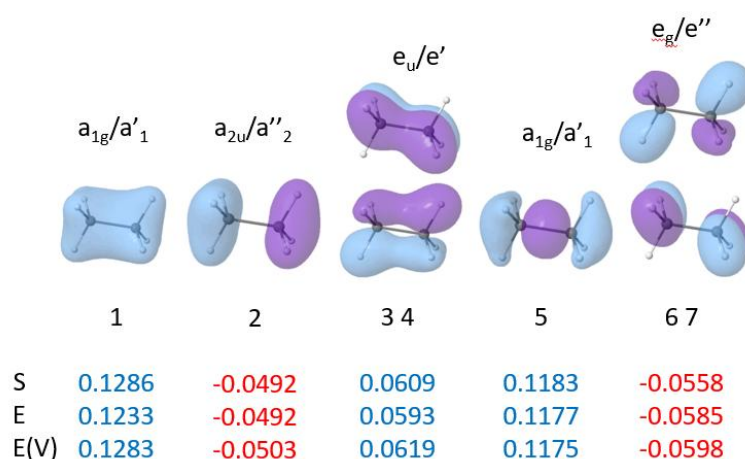


Figure 2. Valence shell dynamic orbital forces (DOF) of optimized staggered (S) and eclipsed (E), vertical eclipsed (E(V)) ethane with respect to H₃C-CH₃ distance (a.u.). Only the MOs of the S conformer are represented.

Regarding the two degenerate π couples, the staggered structure S, compared to vertical E(V) one has less bonding 3-4 MOs (DOF = 0.0609 a.u. vs. 0.0619 a.u.) and less antibonding 6-7 ones (-0.0558 a.u. vs. -0.0585 a.u.), in qualitative agreement with Fig. 1 (a). Nevertheless, due to hyperconjugation, the global (3-4-6-7) interaction has a bonding balance for both S and E(V). The relaxed E structure essentially differ from E(V) by a longer CC distance which moderates these interactions, as well bonding as antibonding. Also, the two σ MOs a_{1g} are more bonding in S than in E due to shorter CC bond.

In order to compare the roles of the MOs in the conformation preference, we report for each of them (Figure 3), the force difference $\text{DOF}(S) - \text{DOF}(E)$ between the staggered and the eclipsed conformations: (a) adiabatic E and (b) vertical EV: a positive value thus means that the corresponding MO favours the S conformation. Figure 3(a) shows that all MOs favour the S conformation with respect to adiabatic E, except MO 2 which has no significant effect, and that MO 1 of σ type plays an important role. By contrast (Figure 3(b)), due to a greater overlap in EV than in E, MOs 3 and 4 slightly favour the vertical eclipsed form, whereas 6 and 7 strongly disfavour it. As a result, the S preference is essentially due to a decrease of MO 6-7 repulsion.

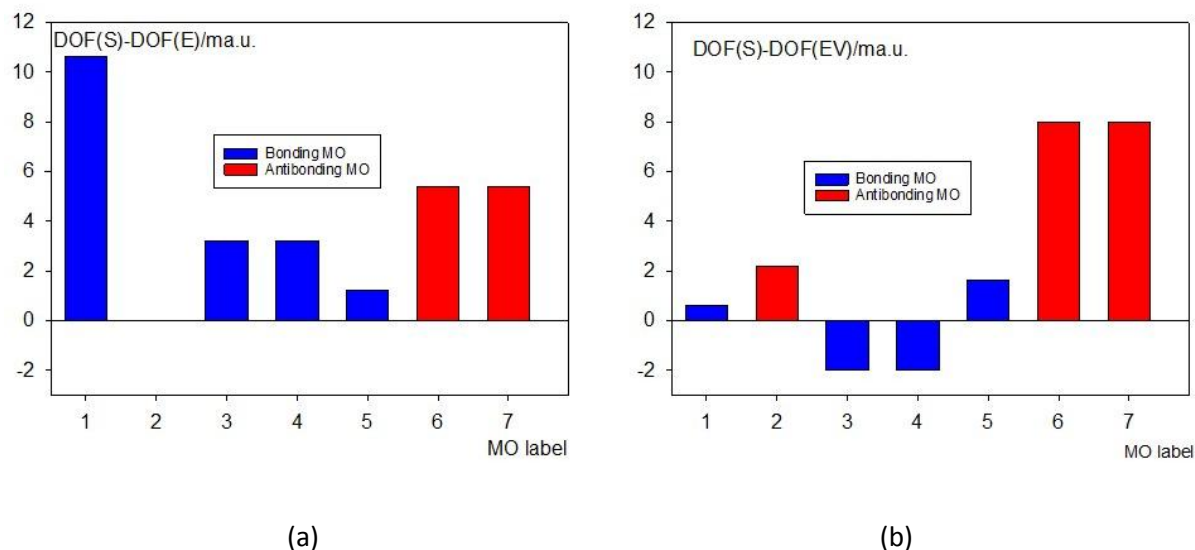


Figure 3. Differences (10^{-3} a.u.) $\text{DOF}(S) - \text{DOF}(E)$ of orbital forces with respect to the $\text{H}_3\text{C}-\text{CH}_3$ distance for each valence shell MO between S and E conformations; (a) adiabatic E structure; (b) vertical EV structure. (A positive value means that the MO favours the staggered conformation.)

4.2. Sum of orbital forces as an index of bond strength; decompositions into attractive/repulsive and σ/π components

We will now consider the variations of the sum Σ_t (Equation 2) as an index of total $\text{CH}_3\text{-CH}_3$ bond strength during adiabatic and vertical rotations. This quantity was decomposed into attractive Σ_b and repulsive Σ^* components (Equation 3). We report (Figure 4) for each of these cases the differences $\Delta\Sigma = \Sigma(\theta) - \Sigma(E)$ as functions of $\theta = \text{H-C-C-H}$ dihedron (a positive value thus favours the θ conformer over the E one ($\theta = 0^\circ$)).

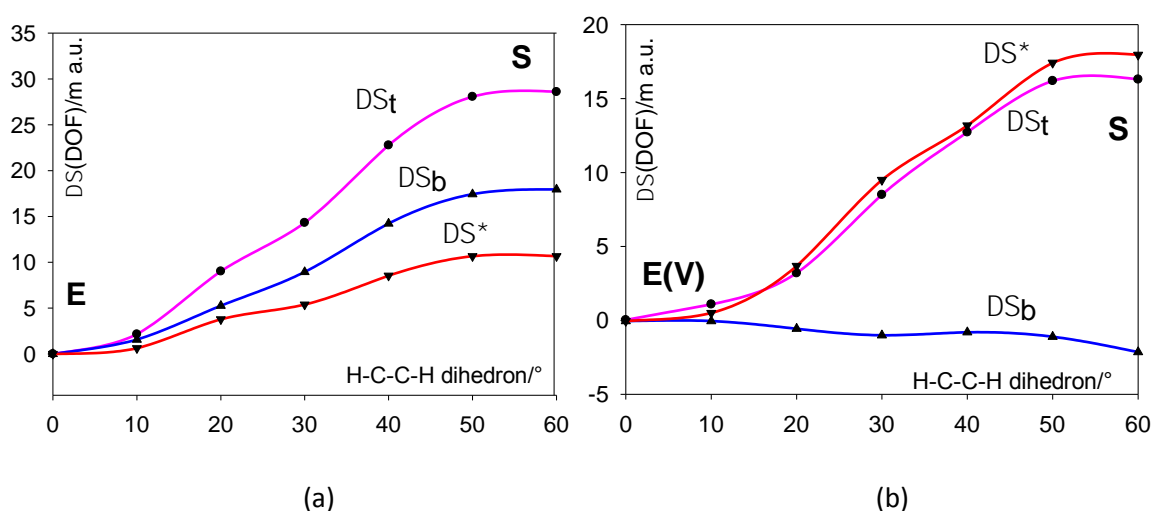


Figure 4. Variation of the sums of orbital forces (m a.u.) along $\text{CH}_3\text{-CH}_3$ as a function of the H-C-C-H dihedron with respect to the eclipsed (E) conformer: (a) adiabatic (optimized geometry); (b) vertical rotation; dots: total sum $\Delta\Sigma_t$; triangles up: sum of bonding MO (attracting) forces $\Delta\Sigma_b$; triangles down: sum of antibonding (repulsive) forces $\Delta\Sigma^*$.

(i) From Fig. 4(a) and Table 1 for the adiabatic rotation, it appears that the stabilization of the S conformer, reflected by an increase of Σ_t , originates mainly in an increase (4.6 %) of attracting forces Σ_b . It is also favoured, in a lesser extent, by a decrease (2.6 %) of repulsive ones Σ^* , yielding an approximate attractive/repulsive participation ratio of 2:1.

(ii) By contrast, in the vertical rotation, the S preference (Figure 4(b) and Table 1) is only due to a decrease of repulsive interactions (4.5 %), so we can understand that the C-C distance elongates to release the repulsion in the E structure. The variation of attractive forces is weak (-0.5 %) and seems to slightly favour the eclipsed conformer.

Table 1. Sums Σ of DOFs (a.u.) and relative differences of $\Delta\Sigma = \Sigma(S) - \Sigma(E)$ (a positive $\Delta\Sigma$ favours the S conformer): S and E, fully relaxed structures; E(V) vertical eclipsed structure; Σ_t total DOF sum; Σ_b bonding MO DOF sum; Σ^* antibonding MO DOF sum; Σ_σ σ -type MO (a symmetry) sum; Σ_π π -type MOs (e symmetry) sum; ΔE : energy barrier (kcal/mol, H-F/aug-cc-pvQZ).

	H ₃ C—CH ₃					6 C—H	ΔE
	Σ_t	Σ_b	Σ^*	Σ_σ	Σ_π	Σ_t	
S	0.4154	0.7374	-0.3216	0.3954	0.0204	1.7537	
E	0.3868	0.7192	-0.3324	0.3836	0.0032	1.7664	
E(V)	0.3995	0.7392	-0.3398	0.3911	0.0084	1.7579	
	$\Delta\Sigma_t/\Sigma_t$	$\Delta\Sigma_b/\Sigma_t$	$\Delta\Sigma^*/\Sigma_t$	$\Delta\Sigma_\sigma/\Sigma_t$	$\Delta\Sigma_\pi/\Sigma_t$	$\Delta\Sigma_t/\Sigma_t$	
S-E	7.2 %	4.6 %	2.6 %	3.0 %	4.3 %	-0.72%	3.17
S-E(V)	4.0 %	-0.5 %	4.5 %	0.4 %	3.0 %	-0.24 %	3.04

We also report in Table 1 the decomposition of Σ_t into σ and π components (Equation 4). The sum Σ_π of π -type interactions (MOs of e symmetry) is positive, thus globally attractive in all three S, E and E(V) structures, which means that the stabilization by hyperconjugation overcomes the 4-electron repulsion, as already noted in section 3.1.

(i) In the adiabatic rotation, the π -type components are only slightly predominant over σ -type ones (MOs of a symmetry) as indicated by the values $\Delta\Sigma_\pi/\Sigma_t = 4.3\%$ and $\Delta\Sigma_\sigma/\Sigma_t = 3.0\%$. This important σ -type contribution mainly arises from MO 1: this MO increases considerably its attractive power in the S conformation, due to a shorter C-C distance with respect to E, and thus an increased overlap. Indeed, its bonding character is almost the same in the S and vertical E(V) structures which have the same CC distance (cf. fig. 3(a)).

(ii) In the vertical rotation, the S preference is almost exclusively due to the decreased antibonding character of π MOs 6-7, originating from the 4-electron repulsion in Fig.1 (cf. also Fig. 3(b)).

4.3. Long range H...H interactions

A further decomposition of orbital forces can be carried out. For this purpose, MO derivatives has been computed:

- with respect to the C-C distance, keeping H...H distances constant: $\frac{d\varepsilon_i}{d(C-C)}$

- with respect to the H₃...H₃ plane distance, keeping C-C distance constant $\frac{d\varepsilon_i}{d(H_3...H_3)}$

It requires a small variation of HCC angles of a negligible consequence, as it can be verified that, within less than 3 %, we get:

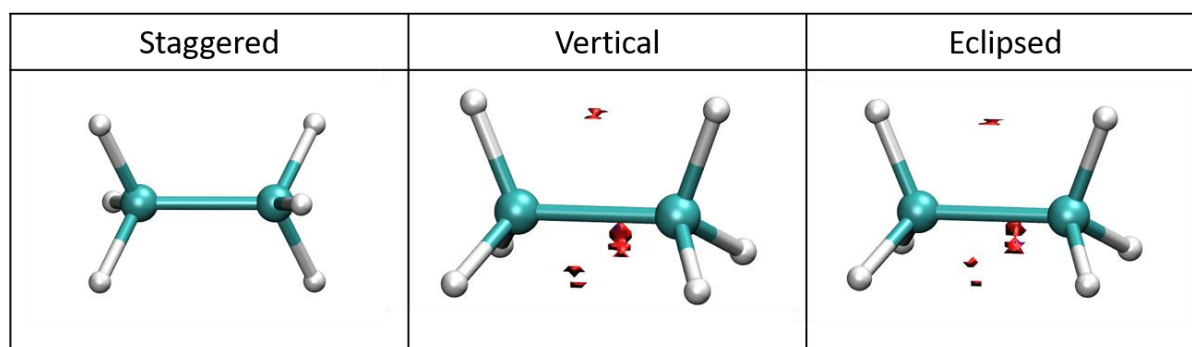
$$\frac{d\varepsilon_i}{d(\text{CH}_3 - \text{CH}_3)} \approx \frac{d\varepsilon_i}{d(\text{C} - \text{C})} + \frac{d\varepsilon_i}{d(\text{H}_3 \cdots \text{H}_3)}$$

The resulting decomposition of Σ_t is reported in Table 2.

Table 2. Sum Σ_t of orbital energy derivatives (a.u.) with respect to various R parameters. (R = CH₃-CH₃, C-C and H₃...H₃) in the S and E conformers.

R	S			E		
	CH ₃ -CH ₃	C-C	H ₃ ...H ₃	CH ₃ -CH ₃	C-C	H ₃ ...H ₃
Σ_t	0.4154	0.4265	-0.0111	0.3868	0.4054	-0.0175

In order to have a localized view of the H₃...H₃ interaction, we have plotted the NCI surfaces which reflect the deformations. Given the long-range nature of these interactions, they are very subtly reflected in the NCI plot. Hence, cutoffs need to be carefully selected in order to choose the interactions we are interested in, and only those. For ethane, $\rho_{\text{max}} = 0.037$ a.u. and $s = 0.8$ is a good compromise (see S.I. for a thorough explanation of this choice). This allows reflecting the H...H non-bonded contacts for the vertical and eclipsed states with respect to the staggered one (see Scheme 1).



Scheme 1. Evolution of NCI surfaces for the different ethane states. Parameters $\rho_{\text{max}}=0.037$, $s=0.8$ were chosen to capture the deviations as seen in the $s(\rho)$ plot (see SI).

In both E and E(V) cases, the interaction H₃...H₃ between hydrogens appears slightly repulsive and favours the S conformer. According to Table 2, the total strengthening Σ_t (S) - Σ_t (E) = 0.0386 a.u. of CH₃-CH₃ bond in the S conformation, with respect to the E one, can be decomposed into 0.0211 a.u. from more attractive C...C interaction and only 0.0064 a.u. from less repulsive H...H interactions. This agrees qualitatively with the NCI pattern, indicating a weak long-range repulsion in both E conformer, too weak to be detected in the S one.

4.4. Decomposition of the energy barrier into bond energy variations.

The energy barrier ΔE does not arise only from the variation of $\text{CH}_3\text{-CH}_3$ bond strength analyzed in the preceding section. We must keep in mind that indeed hyperconjugation stabilizes the system by increasing $\text{BE}(\text{CH}_3\text{-CH}_3)$, but in turn weakens C-H bonds by some electron transfer in C-H antibonding MOs. From Equation 5, the total energy barrier ΔE can be written as:

$$\Delta E \approx -\text{BE}(\text{CH}_3 - \text{CH}_3) \frac{\Delta \Sigma_t(\text{CH}_3 - \text{CH}_3)}{\Sigma_t(\text{CH}_3 - \text{CH}_3)} - 6\text{BE}(\text{C} - \text{H}) \frac{\Delta \Sigma_t(\text{C} - \text{H})}{\Sigma_t(\text{C} - \text{H})} \quad (6)$$

As reported in Table 1, the relative variation $\Delta \Sigma_t / \Sigma_t$ of the sum of orbital forces along $\text{CH}_3\text{-CH}_3$ bond in the S conformation with respect to the E one increases by 7.2 % while the CH bonds are weakened by -0.72 %. Taking $\text{BE}(\text{CH}_3\text{-CH}_3) \approx 90$ kcal/mol and $\text{BE}(\text{CH}) \approx 100$ kcal/mol, Equation (6) yields a total ΔE barrier of 2.2 kcal/mol (+6.5 kcal/mol from $\text{CH}_3\text{-CH}_3$ bond and -4.3 kcal/mol from six C-H bonds). This value, as compared to H-F barrier (3.04 kcal/mol; exp: 2.88 kcal/mol), is rather satisfactory, taking account the approximation of Equation 6, possible errors from the small differences $\Delta \Sigma_t$ and some uncertainty on the intrinsic BE values.

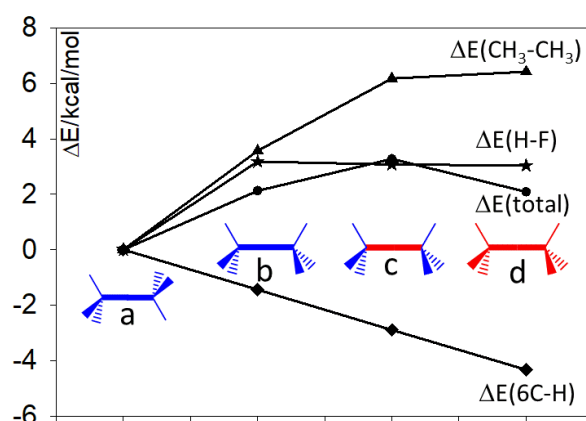


Figure 5. Decomposition of energy variation $\Delta E(\text{total})$ into $\text{CH}_3\text{-CH}_3$ ($\Delta E(\text{CH}_3\text{-CH}_3)$) and C-H ($\Delta E(6\text{C-H})$) bond energies according to Equation 5: a) S optimized structure; b) vertical E; c) E with optimized CC distance; d) fully optimized E; $\Delta E(\text{H-F})$ H-F Energy variation.

The effects of geometry optimization on energy barrier are detailed in Figure 5, according to Equation 5. The following structures have been considered: (a) S, optimized, taken as origin; (b) E, vertical; (c) E, C-C optimized; (d) E fully optimized. These results can be explained as follows.

- The step (a)-(b) consists only in the rotation which increases both 4-electron destabilization of C-C and decreases hyperconjugation which, on the contrary, stabilizes the C-H bonds.
- The step (b)-(c) lengthens the CC distance, with a further destabilization of the CC bond, due now mainly to the decrease of the bonding character of the σ MO 1 (the decrease of hyperconjugation

and 4-electron repulsion are partly cancelling), whereas the decrease in hyperconjugation overlap stabilizes again the C-H bonds.

- The step (c)-(d) is the optimization of C-H bond lengths which are stabilized, with a negligible effect on C-C bonding energy. As already noted^{2a}, the barrier is the same dealing with vertical (b) or adiabatic (d) E structure ($\Delta E(\text{total}) = 2.2$ kcal/mol) due to an almost exact compensation of CC and CH bond energies variations, in agreement with H-F results ($\Delta E(\text{H-F}) = 3.17$ kcal/mol and 3.04 kcal/mol).

This way, the energy barrier appears as mainly due to the interaction of both CH₃ groups which weakens H₃C-CH₃ bond energy, strongly moderated by a stabilization of C-H bonds. This result agrees qualitatively with that reported by Goodman *et al.* using PNBO calculations.^{2a}

5. Comparison with some related X₃A-BY₃ systems

From the preceding section, it appears that the leading interactions between two CH₃ groups, which controls the S preference, can be analyzed using orbital forces. Most notably, it allows the decomposition of the sum Σ_t of orbital forces into attracting (Σ_b) and repulsive (Σ^*) ones and into σ (Σ_σ) and π (Σ_π) type origin. We will compare these four salient parameters of ethane to those of the following related systems: SiH₃-CH₃, SiH₃-SiH₃, CH₃-CF₃ and CF₃-CF₃. All these systems, like ethane exhibit a more or less marked preference for the S conformation (Table 3). Moreover, the rotation barrier for adiabatic and vertical rotations are very close to each other.

Table 3. Energy barriers ΔE (kcal/mol) for adiabatic (A) and vertical (V) rotations.

	CH ₃ -CH ₃	CH ₃ -SiH ₃	SiH ₃ -SiH ₃	CH ₃ -CF ₃	CF ₃ -CF ₃
$\Delta E(\text{A})$	3.07	1.65	1.10	3.44	4.94
$\Delta E(\text{A})$ (exp)	2.88 ^a	1.86 ^b	1.18 ^c	3.18 ^d	4.40 ^e
$\Delta E(\text{V})$	3.18	1.66	1.02	3.55	4.50

^a E. Hirota, Y. Endo, S. Saito, J. L. Duncan, *J. Mol. Spectrosc.* **1981**, *89*, 285-295.

^b L. Borvayeh, I. Ozier, A. Bauder, N. Moazzen-Ahmadi, *J. Mol. Spectrosc.* **2009**, *255*, 122-133.

^c N. Moazzen-Ahmadi, V.-M. Horneman, *J. Chem. Phys.* **2006**, *124*, 194309.

^d S.-X. Wang, J. Schroderus, I. Ozier, N. Moazzen-Ahmadi, V.-M. Horneman, V. V. Ilyushyn, E. A. Alekseev, A. A. Katrich, S. F. Dyubko, *J. Mol. Spectrosc.* **2002**, *214*, 69-79.

^e K. L. Gallaher, A. Yokozeki, S.H. Bauer, *J. Phys. Chem.* **1974**, *78*, 2389-2395.

In Figure 6 and 7 are reported some relative variations $\Delta\Sigma/\Sigma_t$ of sums Σ of MO forces between staggered and eclipsed forms, according to $\Delta\Sigma = \Sigma(\text{S})-\Sigma(\text{E})$. A positive value thus means that the corresponding interaction Σ favours the staggered conformation. Both cases of adiabatic (A) and vertical (V) eclipsed conformations have been considered for each species.

In Figure 6 are compared the sums Σ_b of bonding (attractive) forces and Σ^* of antibonding (repulsive) ones. In Figure 7 are compared the sums Σ_σ of σ (of a symmetry) and Σ_π of π orbital forces (of e symmetry).

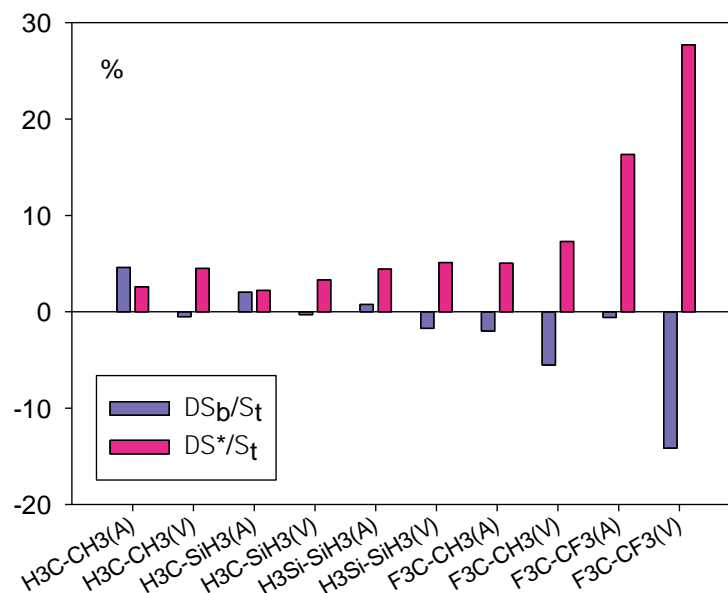


Figure 6. Relative variations (%) of the sums of MO forces: Σ_b bonding (attracting) MOs; Σ^* antibonding (repulsive); a positive value favours the S conformation over the adiabatic(A)/vertical (V) eclipsed one.

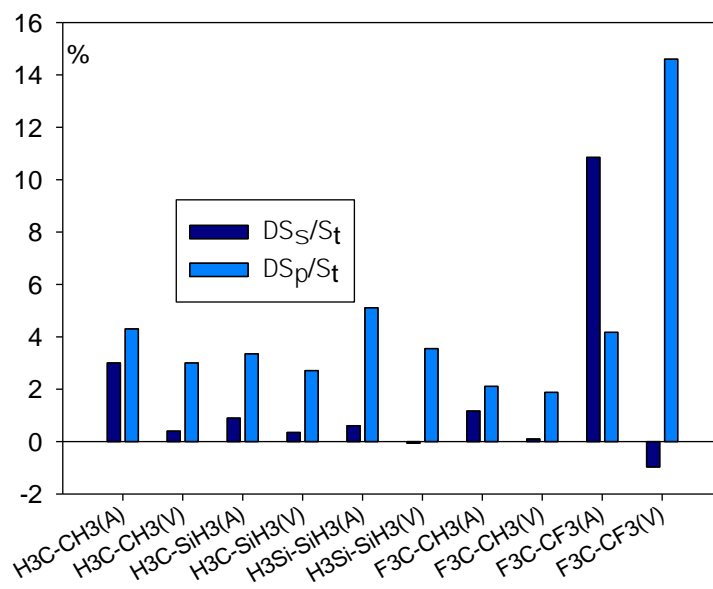


Figure 7. Relative variations (%) of the sums of MO forces: Σ_σ : σ -type (a symmetry) MOs; Σ_π : π -type (e symmetry) MOs; a positive value favours the S conformation over the adiabatic (A)/vertical (V) eclipsed one.

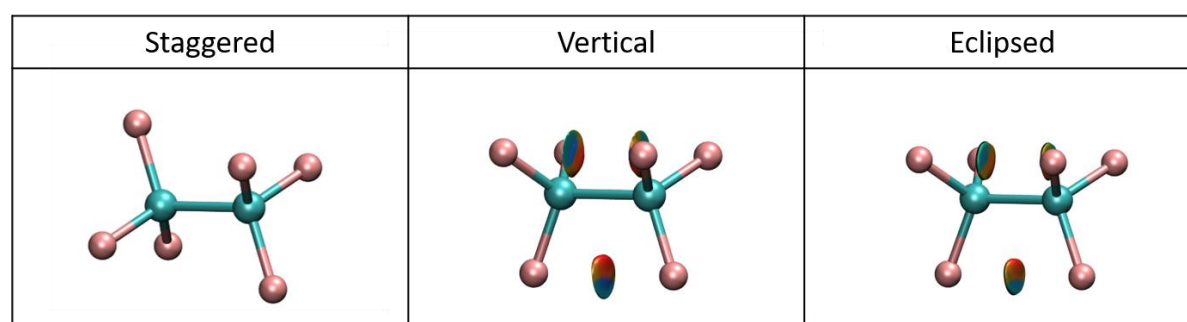
Dealing with adiabatic rotation, C_2H_6 is the only case where attractive forces are dominant to favour the S structure; these forces are slightly lower than repulsive ones in CH_3-SiH_3 and negligible in SiH_3-SiH_3 . This trend can be explained in part by the differences of central bond lengthening in the E conformation. This bond length is increased by 2.3 % in CH_3-CH_3 , 0.6 % in CH_3-SiH_3 and 0.5 % in SiH_3-SiH_3 , thus the bonding character of the σ MO (MO 1 in C_2H_6) is almost the same in the E and V structures of the latter two compounds. This evolution is confirmed by Figure 7, which shows comparable σ and π contributions for ethane, and strongly dominant π interactions in silicon compounds.

In the fluorine compounds CF_3-CH_3 and CF_3-CF_3 , the S preference arises practically from repulsive forces only, and that CF_3-CF_3 appears as the opposite situation to C_2H_6 . The decomposition of the total sum of orbital forces into $C\cdots C$ and $F_3\cdots F_3$ components is displayed in Table 4.

Table 4. Sum Σ_t of orbital energy derivatives (a.u.) with respect to various R parameters. (R = CF_3-CF_3 , C-C, $F_3\cdots F_3$ and C-F) in the S and E conformers.

R	S				E			
	CF_3-CF_3	C-C	$F_3\cdots F_3$	6C-F	CF_3-CF_3	C-C	F_3-F_3	6C-F
Σ_t	0.8081	1.0293	-0.2164	4.7155	0.6879	0.9472	-0.2667	4.7573

As expected from the presence of fluorine lone pairs, the $F_3\cdots F_3$ interaction is strongly repulsive, as compared with $H_3\cdots H_3$ in ethane. Their contribution to total $CF_3\cdots CF_3$ interaction is of the same order of magnitude as the $C\cdots C$ one. This can be visualized in Scheme 2, where NCI surfaces have been plotted at $s = 0.6$ to highlight conformational interplays. In this case, the thin repulsive surfaces of ethane are replaced by well-defined interaction surfaces highlight the non-bonded $F\cdots F$ contacts. Contrary to ethane, in this case the strong repulsive interactions can explain alone the preference for the staggered conformation. Note that for higher s cutoffs, the $F\cdots F$ interactions also appear, in this case both inter and intramolecular (see Fig S2 in SI).



Scheme 2. Evolution of NCI surfaces for the different C_2F_6 states. Parameters $p_{max}=0.04$, $s=0.6$ were chosen to capture the deviations as seen in the $s(\rho)$ plot (see SI).

A weakening of the C-F bonds in the S conformer with respect to the E one is observed, indicating again a significant electron transfer towards C-F antibonding MOs

6. Concluding remarks

As noted in the Introduction, previous works based on MO analysis lead to conflicting results concerning the origin of ethane conformation. Dealing with NBO, the cancelling of empty σ^*_{CH} MOs allowed the evaluation of the weight of hyperconjugation with respect to the repulsion of the filled σ_{CH} ones.² These authors concluded that this interaction was dominated by hyperconjugation, but this term was considered overestimated in subsequent work.^{5a} On the basis of VB calculations including hyperconjugation mesomeric forms^{5b}, it was concluded, on the contrary, to the prominence of repulsive interactions. In the present work, the use of delocalized MOs does not allow to isolate the interactions of C-H bonds which are distributed over all valence MOs, but is able to quantify the total relative attractive and repulsive interactions, their distribution on each MO and on σ/π sets. If we assume that the fictitious vertical eclipsed conformer essentially differs from the staggered one by pure electron and nuclei forces, our results indicate that repulsive forces of π (e) symmetry are nearly the only responsible of the conformational preference. If we consider now the real, geometry relaxed, eclipsed form, the conformation preference arises, on the contrary, mainly from attractive forces (about twice repulsive ones), with almost equal σ and π origins. In addition, by decomposition over bond energy we show that rotation barrier is due to the weakening of the CC bond of CH ones in the 3:2 ratio, which agree with previous results obtained from a different method.³

In related molecules ($\text{SiH}_3\text{-CH}_3$, $\text{SiH}_3\text{-SiH}_3$, $\text{CH}_3\text{-CF}_3$ and $\text{CF}_3\text{-CF}_3$), the S preference is due mainly to the variation of repulsive forces. In hexafluoro ethane, strong repulsive $\text{F}\cdots\text{F}$ long-range interactions are revealed by NCI and orbital forces.

-
- ¹ (a) J. P. Lowe, *J. Am. Chem. Soc.* **1970**, *92*, 3799-3800; (b) R. F. Quijano-Quiñones, M. Quesadas-Rojas, G. Cuevas, G. J. Mena-Rejón, *Molecules* **2012**, *17*, 4661-4671.
- ² (a) L. Goodman, H. Gu, V. Pophristic, *J. Chem. Phys.* **1998**, *110*(9), 4268-4275; (b) V. Pophristic, L. Goodman, *Nature* **2001**, *431*, 565-568; (c) F. Weinhold, *Nature* **2001**, *431*, 539-541.
- ³ J. Fernández Rico, R. López, I. Ema, G. Ramírez, *J. Chem. Phys.* **2003**, *119* (23) 12251-12256.
- ⁴ F. Cortés-Guzmán, G. Cuevas, A. Martín Pendás, J. Hernández-Trujillo, *Phys.Chem.Chem.Phys.* **2015**, *17*, 19021-19029
- ⁵ (a) F. M. Bickelhaupt and E. J. Baerends, *Angew. Chem., Int. Ed.* **2003**, *42*, 4183-4188; (b) Y. Mo and J. Gao, *Acc. Chem. Res.*, **2007**, *40*, 113-119.
- ⁶ F. Weinhold, *Angew. Chem. Int. Ed.* **2003**, *42*, 4188-4194
- ⁷ (a) S. Liu, N. Govind, *J. Phys. Chem. A* **2008**, *112*, 6690-6699; (b) R. O. Esquivel, S. Liu, J. C. Angulo, J. S. Dehesa, J. Antolín, M. Molina-Espíritu, *J. Phys. Chem. A* **2011**, *115*, 4406-4415.
- ⁸ (a) T. Tal, J. Katriel, *Theoret. Chim. Acta* **1977**, *46*, 173-181; (b) P. Chaquin, Y. Canac, C. Lepetit, D. Zargarian, R. Chauvin, *Int. J. Quant. Chem.* **2016**, *116*, 1285-1295; (c) F.M. Bickelhaupt, J. K. Nagle, W.L. Klemm, *J. Phys. Chem. A* **2008**, *112*, 2437-2446; (d) P. J. Robinson, A.N. Alexandrova, *J. Phys. Chem. A* **2015**, *119*, 12862-12867.
- ⁹ Chaquin, F. Fuster, F. Volatron, *Int. J. Quant. Chem.* **2018**, *118*, 25658-25659.
- ¹⁰ a) Y. Yamaguchi, R.B. Remington, J.F. Gaw, H. F. Schaefer III, G. Frenking, *Chem. Phys.* **1994**, *180*, 55-70; b) Y. Yamaguchi, R.B. Remington, J.F. Gaw, H. F. Schaefer III, G. Frenking, *J. Chem. Phys.* **1993**, *98* (11), 8749-8760; c) Y. Yamaguchi, B. J. DeLeeuw, C. A. Richards, Jr., H. F. Schaefer III, G. Frenking, *J. Am. Chem. Soc.* **1994**, *116*, 11922-11930.
- ¹¹ R. Laplaza, J. Contreras-García, F. Fuster, F. Volatron, P. Chaquin, *Comp. Theor. Chem.* **2022**, *1207*, 113505.
- ¹² a) K. Exner, P.v. R. Schleyer, *J. Phys. Chem. A* **2001**, *105*, 3407-3416; b) S. Grimme, *J. Am. Chem. Soc.* **1996**, *118*, 1529-1534
- ¹³ R. Laplaza, J. Contreras-García, F. Fuster, F. Volatron, P. Chaquin, *Chem. Eur. J.* **2020**, *26*, 6839-6845
- ¹⁴ F. Fuster and P. Chaquin, *Int. J. Quant.Chem.* **2019**, *119* (20), e25996.
- ¹⁵ (a) E. R. Johnson, S. Keinan, P. Mori-Sanchez, J. Contreras-García, A. J. Cohen, W.T. Yang, *J. Am. Chem. Soc.* **2010**, *132*, 6498. ; (b) J. Contreras-García, E. R. Johnson, S. Keinan, R. Chaudret, J.-P. Piquemal, D. Beratan, W. J. Yang, *Chem. Theory. Comput.* **2011**, *7*, 625.
- ¹⁶ B. Levy, M. C. Moreau, *J. Chem. Phys.* **1971**, *54*, 3316-3321
- ¹⁷ Gaussian 09, Revision A.01, M. J. Frisch, G. W. Trucks, H. B. Schlegel, G. E. Scuseria, M. A. Robb, J. R. Cheeseman, G. Scalmani, V. Barone, B. Mennucci, G. A. Petersson, H. Nakatsuji, M. Caricato, X. Li, H. P. Hratchian, A. F. Izmaylov, J. Bloino, G. Zheng, J. L. Sonnenberg, M. Hada, M. Ehara, K. Toyota, R. Fukuda, J. Hasegawa, M. Ishida, T. Nakajima, Y. Honda, O. Kitao, H. Nakai, T. Vreven, J. A. Montgomery, Jr., J. E. Peralta, F. Ogliaro, M. Bearpark, J. J. Heyd, E. Brothers, K. N. Kudin, V. N. Staroverov, R. Kobayashi, J. Normand, K. Raghavachari, A. Rendell, J. C. Burant, S. S. Iyengar, J. Tomasi, M. Cossi, N. Rega, J. M. Millam, M. Klene, J. E. Knox, J. B. Cross, V. Bakken, C. Adamo, J. Jaramillo, R. Gomperts, R. E. Stratmann, O. Yazyev, A. J. Austin, R. Cammi, C. Pomelli, J. W. Ochterski, R. L. Martin, K. Morokuma, V. G. Zakrzewski, G. A. Voth, P. Salvador, J. J. Dannenberg, S. Dapprich, A. D. Daniels, Ö. Farkas, J. B. Foresman, J. V. Ortiz, J. Cioslowski, D. J. Fox, Gaussian, Inc., Wallingford CT, **2009**.

¹⁸ (a) J. Contreras-Garcia, E. Johnson, S. Keinan, R. Chaudret, J-P Piquemal, D. Beratan, W. Yang, *J. Chem. Theor. Comp.* **2011**, *7*, 625-632; (b) R. A. Boto, F. Peccati, R. Laplaza, C. Quan, A. Carbone, J.-P. Piquemal, Y. Maday, J. Contreras-Garcia, *J. Chem. Theory Comput.* **2020**, *16*, 7, 4150-4158; (c) R. Laplaza, F. Peccati, R. A. Boto, C. Quan, A. Carbone, J.-P. Piquemal, Y. Maday, J. Contreras-García, *WIREs Journal of Computational and Molecular Modeling* (2020). <https://doi.org/10.1002/wcms.1497>